



GROUTED SPLICE PRECAST COLUMN CONNECTIONS WITH SHIFTED PLASTIC HINGING

H. Al-Jelawy⁽¹⁾, Z. Haber⁽²⁾, K. Mackie⁽³⁾

⁽¹⁾ PhD student, University of Central Florida, haiderucf@knights.ucf.edu

⁽²⁾ Program Manager & Bridge Research Engineer, Genex Systems, zhaber@genexsystems.com

⁽³⁾ Associate Professor, University of Central Florida, Kevin.Mackie@ucf.edu

Abstract

Accelerated bridge construction (ABC) has gained popularity in urban areas where construction risk and traffic delays need to be minimized. The use of prefabricated elements is essential in most ABC projects to meet tight scheduling demands. Due to lack of knowledge regarding non-linear performance of connections, prefabricated substructure elements have been utilized more frequently in areas of low seismicity compared with areas with higher seismic hazard. Connections employing grouted coupler splices are becoming one of the more popular options for some U.S. transportation agencies. Previous studies have shown that precast columns with grouted splice connections behave similar to cast-in-place columns when subjected to non-linear cyclic loading. However, these connections have also been shown to disrupt plastic hinge formation, which results in premature failure and reduced displacement ductility.

This paper presents the preliminary results from an experimental study on precast concrete columns with grouted splice moment connections. The primary goal of the study is to develop new connection details employing grouted splices that exhibit improved seismic performance compared with previously tested connections details. Four 0.42-scale bridge column models were designed based on Caltrans' Seismic Design Criteria with different aspect ratios to represent flexural and flexural-shear dominated configurations. Of the four models, two precast columns were designed such that plastic hinging forms above the grouted couplers. In previous studies, columns employing these couplers exhibited concentrated plastic rotation at the column-footing interface, which resulted in premature bar rupture and reduced ductility. Thus, the proposed design method shifts plastic hinging to a region with higher plastic rotation capacity to increase ductility and improve seismic performance. Precast columns are compared with a corresponding set of cast-in-place column models that establish baseline performance. All four columns were subjected to slow cyclic lateral loading in a single cantilever configuration. Hysteretic force-displacement relationships, damage observation and energy dissipation for the precast models are compared with like results from corresponding CIP column models. Furthermore, quantification of the displacement components that contribute to the total lateral displacement is performed to assess the hinging behavior of the precast column compared with CIP column.

Keywords: Precast; grouted splice; column; ABC; shifted hinge

1. Introduction

1.1. Background and Previous Studies

Accelerated bridge construction (ABC) has become increasingly popular throughout the United States since it offers several advantages compared with conventional construction methods. Some of the advantages include minimizing construction time and project costs, reducing traffic disruption, enhancing construction quality, reducing environmental impacts, and minimizing work zone risk. An essential part of ABC projects is the use of precast (prefabricated) elements. Although precast concrete elements are widely used in regions with varying seismicity, precast substructure elements have seen limited use in regions with high seismicity due to concerns related to seismic performance of connections. Connection regions for precast substructure elements typically coincide with plastic hinge zone that are subject to high deformation demands and damage during ground shaking. To date, there have only been a limited number of studies investigating precast column connections for use in high seismic zones. Marsh et al. [1] provides an excellent summary of the available literature and groups of connections that have been tested or implemented in the field. ABC connections with grouted splice couplers have gathered a great deal of attention from designers and engineers due to their good field tolerates and ease of assembly. However, bridge columns with grouted splice connections have only been subject to a limited number of investigations in the US, as explained in the next paragraph. Nevertheless, research thus far has indicated some performance issues related to this type of connection detail for seismic applications.

The cyclic performance of three large-scale column models was reported by Haber et al. [2], where two columns were precast columns that had grouted splice connections, and the third one was a control cast-in-place (CIP) column model. The precast column employed grouted splices at the base of the precast column shaft and connected directly to the footing; this is the typical configuration for a grouted splice connection (shown in Figure 1). The second precast column employed a precast pedestal one-half column diameter in height separating the footing and the precast column. Footing bar dowels passed through grout-filled corrugated steel ducts within the pedestal and connected with grouted splices at the base of the precast column. Columns were tested using slow cyclic loading in a single cantilever configuration. All specimens showed similar performance in terms of ultimate load capacity and energy dissipation up to 6% drift. However, the precast columns exhibited approximately 40% reduction in displacement ductility capacity compared with the CIP column. The reduction was a result of disrupted plastic hinge formation caused by the added stiffness of grouted splices and pedestal ducts. Strain concentrations formed at the column-footing interface and premature bar rupture occurred in the footings.

A similar study was conducted by Ameli et al. [3] investigated the performance of two half-scale precast bridge columns specimens with grouted splice column-to-cap beam connections. One specimen had a typical column-footing connection detail (grouted splices at the column base). The second precast column employed the grouted splices in the cap beam. Both columns were tested using slow cyclic loading, and were compared with a corresponding cast-in-place column. The measured displacement ductility capacities for the first and second columns were 50% and 42% lower than the corresponding cast-in-place columns, respectively. As noted Ameli et al. [3], the behavior and failure of the first column was similar to that observed by Haber et al. [2]. The second precast column (grouted splices in the cap beam) showed improvement compared to the first column (typical connection). Well-distributed hinging was achieved by moving the splices into the cap beam. However, it should be noted that this detail could create constructability issues related to congestion of reinforcement in the cap beam.

Tazarv and Saiidi [4] investigated the seismic performance of a single precast column model that employed grouted couplers within the plastic hinge region. The precast model tested employed the same geometry, coupler type, and reinforcement ratios as the columns tested by Haber et al [2]. The goal of the research was to improve the seismic performance of precast column connections employing grouted couplers. The precast column model was connected to a cast-in-place footing atop a pedestal one-half column diameter in height. The longitudinal reinforcing bars that passed through the pedestal were debonded from concrete using duct tape to improve plastic rotation and displacement ductility capacity, but were fully bonded within the footing and within the grouted couplers. The column was tested using slow cyclic loading in a single cantilever

configuration. Compared with the CIP model tested by Haber et al [2], the precast column model only exhibited a 15% reduction in ductility, which was greatly improved compared with previously tested columns with grouted couplers.

In summary, the majority of precast columns with grouted splice connections have exhibited reduced ductility compared with corresponding cast-in-place columns. Although improved seismic performance has been found by using alternative design details, there can be constructability issues associated with such design details. For instance, placement of couplers in the capacity-protected member may result in reinforcement congestion, and employing pedestals require more onsite construction time. Given the demand for ABC and popularity of grouted splice connections, there is still a need to develop improved details and design methods.

1.2. Objective and Scope

The objective of the study is to present and validate a new connection detail for precast columns with grouted splices with improved performance compared with previously tested details. The proposed connection detail employs shifted plastic hinging (SPH) to relocate the critical column section above the grouted splice region. Shifted plastic hinging has been studied previously for new building construction [5], and in bridge applications, SPH has been primarily used for repair and retrofit of earthquake-damaged columns [6-8]. The study includes experimental testing and analysis of six large scale circular bridge column models. This paper only presents some of the preliminary experimental results from four of the column models. Two sets of columns were tested, one with aspect ratio (AR) of 4.0 and the other with AR of 2.5. In each set, one column was a conventional cast-in-place model used as a control, and the other column was a precast column utilizing grouted splices.

2. Experimental Program

2.1. Design Concept

The plastic hinge locations for a conventional bridge column, a column with a typical grouted splice connection, and a column with the proposed SPH detailing are shown in Fig. 1. In the conventional column, well-distributed plasticity will occur at the base of the column producing adequate displacement ductility capacity. In the typical grouted splice detail, the majority of plasticity is concentrated at the interface between the column and the adjacent capacity-protected member. The concentration of plasticity limits plastic rotation and ductility capacities. In the proposed detailing, the plastic hinge zone is shifted above the sleeve region to realize improved plastic rotation capacity.

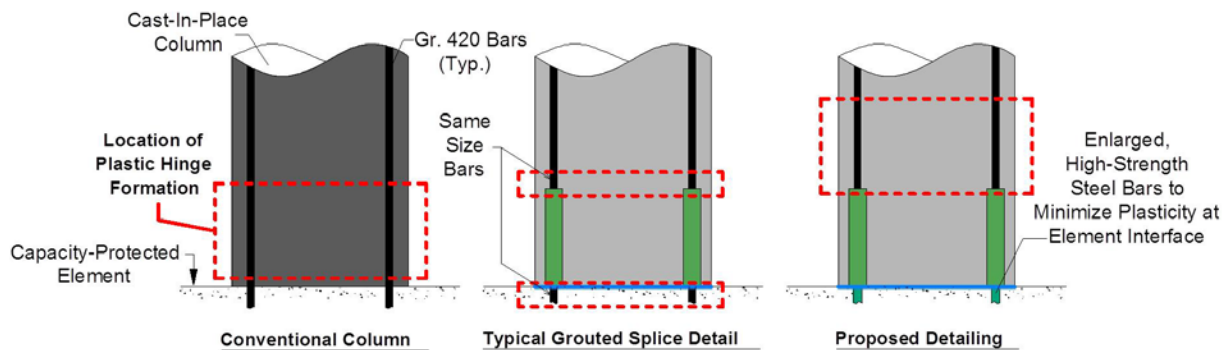


Fig. 1 - Comparison of Hinge Formation Locations

The shifted plastic hinge location is achieved by increasing the plastic moment capacity of the section at the column-footing (or column-cap) interface relative to the section located above the grouted splices. To achieve this using currently-available grouted splice technology, a transition splice detail can be employed along with high-strength reinforcing bars in the capacity-protected element. Transition splicing refers to using a smaller bar in one end of the splice and a larger bar in the other. That is, for example, if the section above the

grouted splices was designed using Gr. 420 M25 bars then the section at the interface of the capacity-protected member would employ Gr. 690 (or Gr. 830) M28 bars. In the example case, an M28 coupler sleeve would be used to join the two different bar types. Larger, higher strength bars at the column base increase the yield moment at that section such that the critical section exists above the grouted splices. The primary goal of the purpose of this detail is to develop well-distributed plastic hinging above the splice region, and to reduce excessive damage in the capacity-protected members.

2.2. Specimen Design and Details

Four 0.42 scale reinforced concrete bridge column models were fabricated to evaluate the shifted plastic hinge design. Two sets of columns were used: one with AR = 4.0 and the other with AR = 2.5. Each set consisted of one cast-in-place (CIP) column and one precast column with grouted couplers. Column details are shown in Table 1. For example, the pre-cast column with AR = 4.0 is designated G-40-1. The column models were designed according to the Caltrans' Seismic Design Criteria (SDC) [9], to evaluate the behavior of the proposed SPH design detail.

Table 1 - Details of the columns

Column ID		D (mm)	L/D	Longitudinal Reinforcement Ratio (%)	Transverse Reinforcement Ratio (%)	Pitch (mm)
CIP	C-40-1	508	4	1.95	0.738	38
Precast	G-40-1	508	4	1.43	0.738	38
CIP	C-25-1	508	2.5	1.43	0.485	57
Precast	G-25-1	508	2.5	1	0.492	57

Fig. 2 shows the basic geometric and material properties used in the design of columns with AR = 4.0; the analysis procedure for columns with AR = 2.5 was similar and is not discussed in detail in this paper. The conventional column, C-40-1, used 10 – M22 Gr. 420 longitudinal bars and a MW29 smooth wire spiral at a 38-mm pitch. The calculated target displacement ductility for C-40-1 was $\mu_c = 6.9$. The precast column, G-40-1, was designed to achieve the same plastic lateral load capacity as the conventional column assuming the critical section occurs above the spliced region (neglecting the flexibility of grouted splice region and column-footing interface). The critical section, denoted “G1”, was reinforced with 10 – Gr. 420 M19 longitudinal bars. A lower reinforcement ratio could be used given the shorter moment arm (L_{Eff}) between the tip of the column and the critical section. G-40-1 used the same transverse reinforcement detailing as C-40-1. This was done to assess the applicability for using emulative design procedures for columns with grouted spliced and shifted plastic hinging. Section G2 employed 10 – Gr. 690 M22 longitudinal bars. Grouted splices sized for M22 bars were used to transition M19 bars in section G1 with M22 bars in section G2. Fig. 3-a depicts the design details of G-40-1 column.

For column G-40-1, a series of moment-curvature analyses were conducted using OpenSees. Section analysis showed that when the plastic moment is reached at critical section above the grouted splices (section G1), the moment at the base of the column (section G2) is lower than the expected yield moment. Thus, the base section should remain essentially elastic. The maximum calculated stress in the high-strength bars was 580 MPa, which is lower than the maximum expected tensile strength of ASTM A706 Gr. 420 bars ($f_u = 665$ MPa). Most grouted splices available in the US market are designed to be used with ASTM A615 and A706 bars. Thus, the maximum expected stress level in the high-strength bars must be less than the expected ultimate tensile strength of the bar type designed to be used with the splice. This is to prevent bar pullout failure or coupler sleeve fracture.

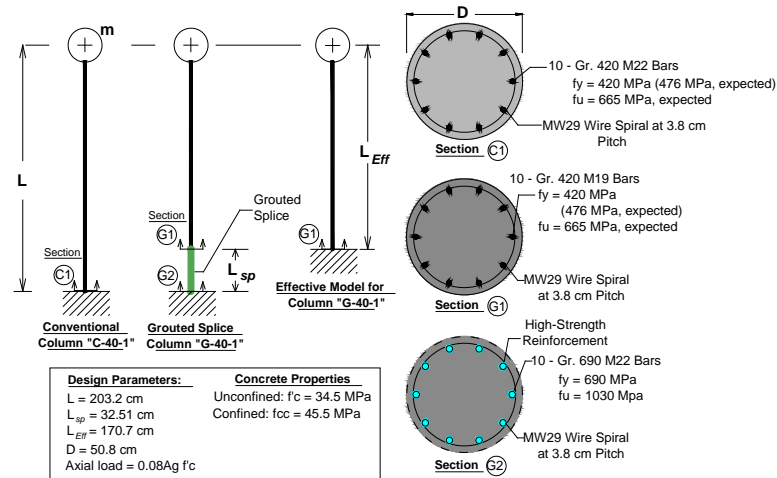


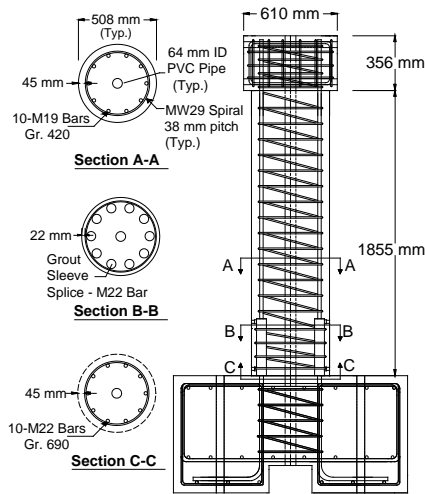
Fig. 2 - Design Parameters and Properties of Columns with AR=4

The conventional column with AR=2.5, C-25-1, was reinforced with 10 – M19 Gr. 420 longitudinal bars and transversely with a MW29 smooth wire spiral at a 57-mm pitch. The calculated target displacement ductility was $\mu_c = 7.6$. The corresponding precast column, G-25-1, was reinforced with 10 – M16 Gr. 420 longitudinal bars in the critical section (above the splice region) and 10 – M19 Gr. 690 longitudinal bars below the splice region (footing) (refer to Fig. 3-b). M19 grouted splices were used to transition the longitudinal bars in the column shaft with the bars in the footing.

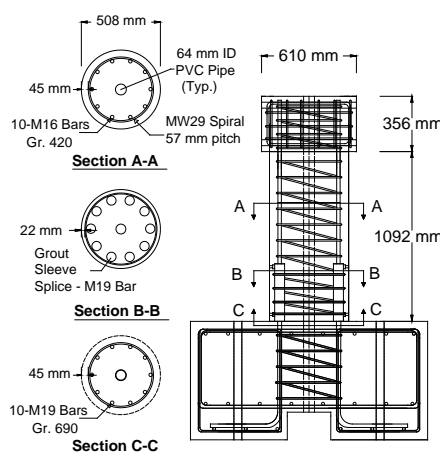
Four materials were used to construct the column models: conventional concrete, mild reinforcing steel, high strength reinforcing steel and SS Mortar grout. Column models were constructed in two stages. Footing concrete was cast first, followed by the column shaft. Mild and high strength reinforcing steel were ASTM A615 Gr. 420 and ASTM A1035 MFX Gr. 690 steel bars, respectively. SS mortar grout was the proprietary grout that should be used with the sleeves provided by Splice Sleeve Japan (SSJ) Inc. The concrete strength of the column and footing on the day of testing was about 65.5 MPa and 52.5 MPa for all models. The yield and ultimate strength of the mild steel bars ranged between 449 MPa to 469 MPa and 711 MPa to 738 MPa, respectively. The yield and ultimate strength for high-strength steel bars ranged between 870 MPa to 897 MPa and 1118 MPa to 1228 MPa, respectively; yield was determined using a 0.2% offset. On the day of testing, the compressive strength of the SS mortar grout ranged between 123 MPa to 129 MPa for models G-40-1 and G-25-1, respectively.

2.3. Instrumentation and Testing

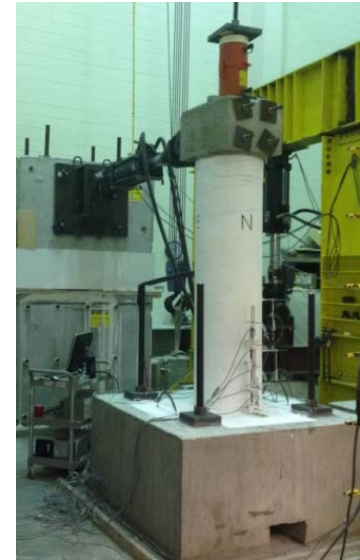
The column models were tested at the Structures Laboratory at the University of Central Florida. The models were tested in a single cantilever configuration using a 445 kN servo-controlled hydraulic actuator. The actuator was mounted on a reaction wall that was post-tensioned to the laboratory strong floor using high-strength steel rods. A photo of the test setup is shown in Fig. 3-c. Columns were tested using a cyclic, quasi-static lateral loading protocol that was applied using drift-based displacement control. Drift levels of 0.25, 0.5, 0.75, 1, 2, 3, 4, 5, 6, 8 and 10% were applied in succession or until failure, which was characterized by a 20% loss of lateral load capacity. Two full cycles were applied for each drift level. The applied axial load was 560 kN, which corresponds to an axial load ratio or axial load index (ALI) of 0.08; ALI is defined as the ratio of axial load divided by the product of column cross sectional area and concrete compressive strength. Axial loading was applied using double acting hollow-core hydraulic jack. The hydraulic pressure was maintained using a relief valve, and the axial load was monitored using a pressure transducer.



(a) Precast Column (G-40-1)



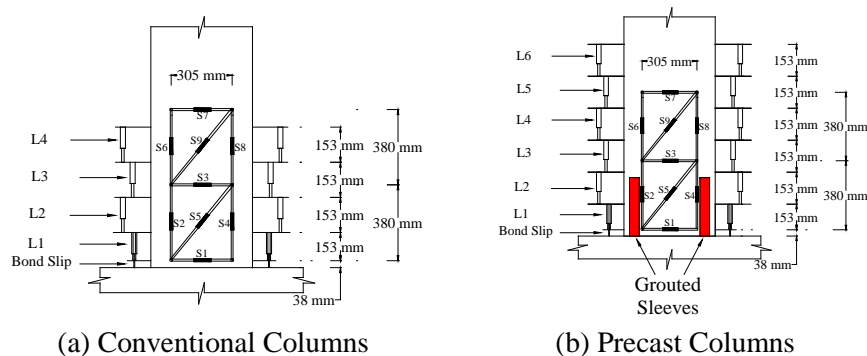
(b) Precast Column (G-25-1)



(c) Test Setup

Fig. 3 – Precast Columns Design Details and Test Setup

All column models were instrumented internally with strain gauges. The strain gauges were installed on the reinforcement cage of the column shaft and the footing at different layers ranging from below the footing surface and through the plastic hinge region. The column models were instrumented externally with linear variable displacement transducers (LVDTs) to measure curvatures, bond-slip, and shear deformations within the expected plastic hinge zone. The configuration of these instruments is shown in Fig. 4.



(a) Conventional Columns

(b) Precast Columns

Fig. 4 - Schematics of Curvature and Shear Instrumentations

4. Experimental Results and Discussion

4.1. Observed Damage

Fig. 5 depicts and compares the damage progression for columns with $AR = 4$ at 4% and 8% drift. Before 4% drift, hairline flexural cracks developed for both columns. At 4% drift (Fig. 5), more hairline flexural cracks appeared in both columns. Flexural cracks localized for both columns at different heights. For C-40-1, wide flexural cracks localized near the column-footing interface (Fig. 5-a), and for G-40-1 the localization of flexural cracks was primarily at or above the sleeve location (Fig. 5-b). The difference in observed damage can be attributed to several reasons. First, the column was detailed such that the critical section exists above the sleeve. Second, strain penetration of the column bars into the grouted couplers contributes to the wide flexural crack at

the top sleeve. Third, during construction of the precast columns a rubber cap is used on the top end of the sleeve preventing column concrete from entering the sleeve during casting. This cap debonds the longitudinal bars over a very short length (approximately 13 mm) resulting in larger concentrated rotations for a given applied load, which increases the crack width.

Another noticeable difference between the two columns was the amount of cracking in the footing. C-40-1 developed cracks in the footing that became significant at higher drift levels as a result of strain penetration, while G-40-1 did not exhibit such cracks until failure. By 8% drift (Fig. 5-c, d), significant difference in spalling height was observed between the two columns. C-40-1 had spalled concrete within the first 305 mm from the footing surface, while G-40-1 had spalled concrete over the first 660 mm above footing surface. This difference is not unexpected given that G-40-1 was designed to develop damage above the sleeve location. Although concrete spalled within the coupler region, the damage did not penetrate into the core concrete. At failure, both columns exhibited bar buckling and fracture of transverse reinforcement as result of bar buckling. Unlike C-40-1, G-40-1 had longitudinal bar fracture occur during the first push to -8%. As expected, the damage that occurred in C-40-1 was concentrated near the column-footing interface, whereas damage in G-40-1 was concentrated above the coupler region.

Damage progression for columns with AR = 2.5 at 4% and 5% drift is shown in Fig.6. Until 3% drift, both columns had developed several flexural and shear cracks. At 4% drift, significant spalling can be observed for both columns. The spalled concrete height for C-25-1 was 228 mm above the footing surface, and 355 mm for G-25-1. The increased height of spalling in G-25-1 is not unexpected. Shear cracks were wider in G-25-1 than in C-25-1 (refer to Fig. 6-c,d) due to the presence of the coupler region that stiffened the base of the column and shortened the effective cantilever length. Strain penetration developed in the footing of C-25-1, which caused delamination of concrete at the surface of the footing. This was not noticeable in G-25-1 due to presence of high-strength bars with enlarged sizes that led to elastic behavior at the section below the sleeves.

By the end of 5% drift, C-25-1 did not exhibit significant changes in apparent damage, while G-25-1 showed substantial changes in damage progression. Damage penetrated the concrete core above the coupler zone. Bar buckling occurred on the north side of the column causing the couplers to push away from the core concrete. Spalling of cover concrete can be observed in the south side of G-25-1 model up to 609 mm above the footing surface. At failure, both columns exhibited bar buckling and fracture of transverse reinforcement as result of bar buckling. Unlike C-25-1, G-25-1 had two longitudinal bars fractured during the first push to 6% and one longitudinal bar fracture during the first pull to 6%.

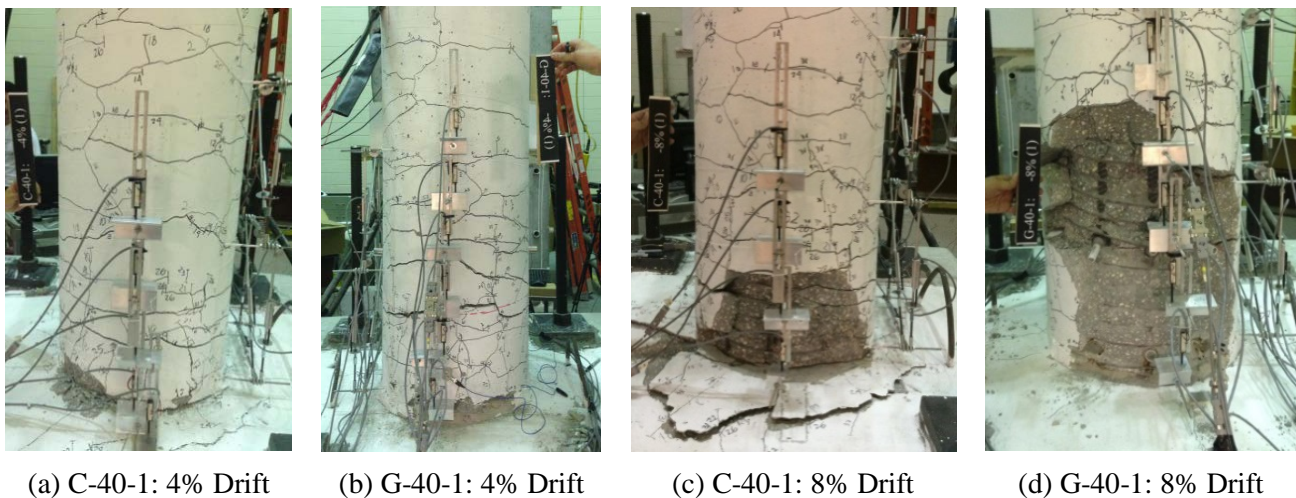


Fig. 5 – Observed Damage in Models with AR = 4.0

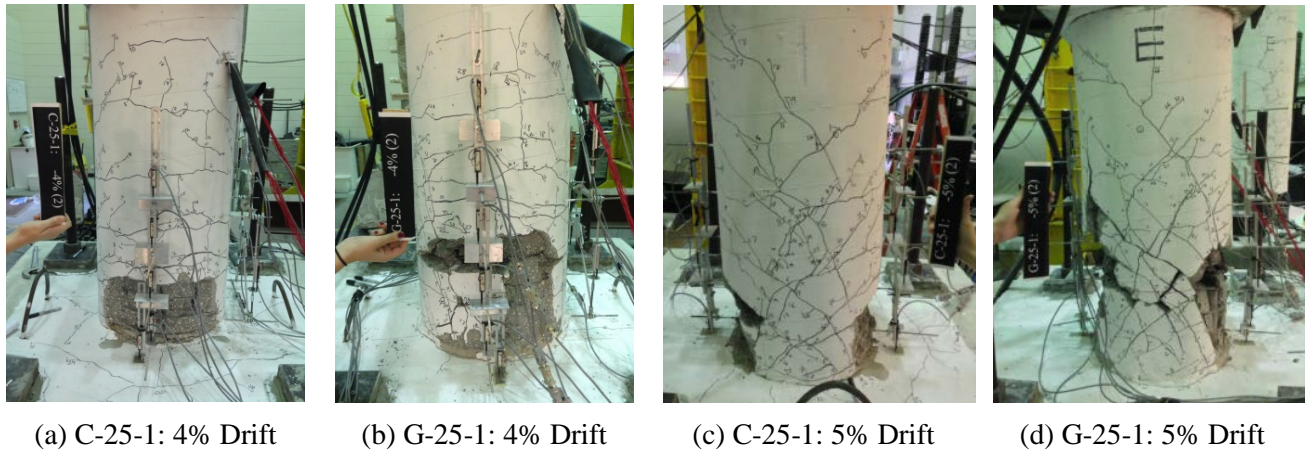


Fig. 6 – Observed Damage in Models with AR = 2.5

4.2. Load-Displacement Relationship

The hysteresis loops for columns with AR = 4 and AR = 2.5 are shown in Fig. 7 and Fig. 8, respectively. All columns exhibited stable hysteresis behavior. For columns with AR = 4 (Fig. 7), the hysteresis behavior for G-40-1 showed less lateral load capacity compared to C-40-1, which was due to a slight construction error. G-40-1 was designed to have 45 mm concrete cover above the sleeve location, but was constructed with 57 mm of concrete cover. The change in cover led to less confined concrete area, shorter distance between the neutral axis and the tension steel, and slightly lower section capacity. The expected and measured reduction in lateral capacity was 15.25% and 16.7%, respectively, due to cover increase..

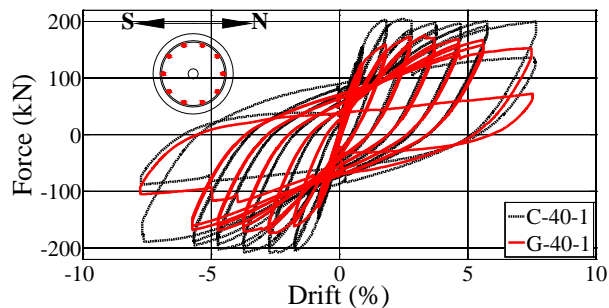


Fig. 7 - Hysteresis Loop of Columns with AR=4

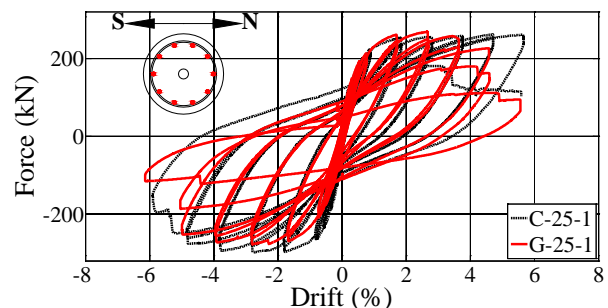


Fig. 8 - Hysteresis Loop of Columns with AR=2.5

For columns with AR = 2.5, both models achieved approximately similar lateral load capacity. The hysteresis behavior for C-25-1 exhibited more lateral load capacity in the pull direction due extra concrete cover in the compression zone. During construction, the reinforcing steel cage was unintentionally shifted 25.4 mm towards the North side of the column. The precast column model, G-25-1, exhibited less ductile behavior than the control model (C-25-1). This can be attributed to the precast model undergoing more shear deformation than the control model. The stiffened coupler region in G-25-1 caused the column to have a shorter effective aspect ratio that resulted in higher shear intensity and deformation compared with C-25-1. It can be observed from the hysteresis loops of G-25-1 that there is noticeable degradation at high drift levels compared to C-25-1 model. This was caused by shear degradation of concrete from widening of the inclined shear cracks and reduced aggregate interlock along the cracks [10].

Pushover curves for columns with AR = 4 and AR = 2.5 are shown below in Fig. 9 and Fig. 10, respectively. For each column, the backbone curve was obtained by taking the peak values of hysteresis loop for

both push and pull sides and averaging them. The elasto-plastic curve (EP curve) was calculated such that the area under the EP and backbone curves had equivalent areas. The elastic portion of EP curve was selected to pass through the “first yield point” on the backbone curve. The EP curve was used to determine displacement ductility. Columns with AR = 4 and AR = 2.5 showed a reduction of 8% and 19% in displacement ductility compared with their corresponding CIP models, respectively. Compared with previous grouted splice studies [2, 5, 6], the precast columns in this study performed very well, especially G-40-1.

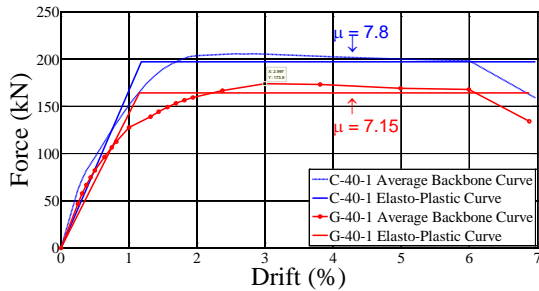


Fig. 9 - Average Force-Displacement Backbone Curve for columns with AR=4

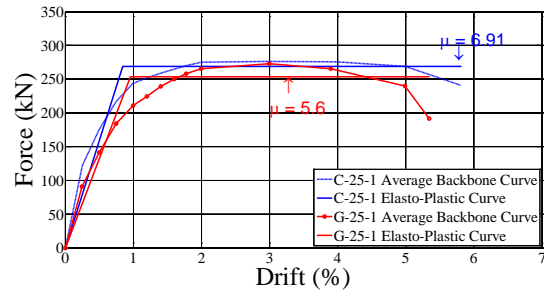


Fig.10 - Average Force-Displacement Backbone Curve for columns with AR=2.5

4.3. Energy Dissipation

As discussed earlier, the hysteresis loops of G-40-1 model showed lower lateral capacity than C-40-1. To make sure that this difference in capacities is not related to performance behavior of the precast column, the energy dissipation of both CIP and precast models was computed. Energy dissipation of the column models is presented in terms of the equivalent viscous damping ratio (ζ). The ratio ζ normalizes the energy dissipation with respect to the effective stiffness, allowing an effective comparison between specimens without the effect of having different lateral capacities. Ratio ζ was calculated using Eq. (1), where E_D is the energy dissipation per cycle or the area enclosed by one hysteresis loop, k_{eff} is the effective stiffness from Eq. (2), and d_{max} and d_{min} are the maximum positive and negative displacements of the hysteresis loop, respectively. F_{max} and F_{min} are the associated forces at d_{max} and d_{min} , respectively. Fig. 11 shows ζ at each drift level for all columns up to 6% and 5% drift ratios for columns with AR = 4 and AR = 2.5, respectively. It was because the columns had capacity degradation and failure after these drift levels. The damping ratios shown are averages from the 1st and 2nd cycle of each drift ratio. The dissipated energy is very low up to 1% drift level (prior to steel yielding). After that it begins to increase due to yielding of reinforcing bars. G-40-1 had a 6% more energy dissipation than C-40-1 and which indicates that higher strain was developed in the longitudinal bars of that column. On the other hand, G-25-1 achieved a 8% less energy dissipation than C-25-1 which indicates lower strain was developed in the bars of that column.

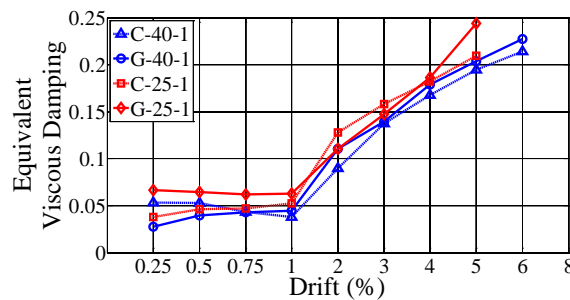


Fig. 11 - Average Equivalent Viscous Damping Ratio for Columns

$$\zeta = \frac{E_D}{2\pi k_{\text{eff}} \cdot d_{\text{max}}} \quad (1)$$

$$k_{\text{eff}} = \frac{F_{\text{max}} - F_{\text{min}}}{d_{\text{max}} - d_{\text{min}}} \quad (2)$$

4.4. Displacement Contributions

Damage observation of column models showed how the plastic hinge was shifted above the sleeve. Although visual damage could be enough indicator that SPH works effectively for grouted splice column connection with flexural dominant behavior, it was not clear enough for G-25-1 column. Therefore, there is a need to isolate the different components of displacements that contribute to the total lateral column displacement. Doing so should shed more light on the behavior of the plastic hinging.

Total displacement of the column tip is the sum of: flexural, shear and strain penetration deformations. Fig. 12 depicts the individual components of the column tip displacement for all columns in the study for the 1st push cycles only which is considered to be representative of other cycles. The results are shown up to 4% drift where reliable data are considered. For C-40-1 model, strain penetration in the footing contributes the most (30-60%) to the overall displacement observation of column models. Flexural contributions decrease with the column height from level L1 to L4 (refer to Fig. 4). This is a typical hinging behavior of a CIP column.

On the other hand, plastic hinging behavior of G-40-1 model was different. Strain penetration in the footing still had a significant contribution to the overall column displacement but less than that observed in C-40-1. This was because the high-strength bars did not exhibit nonlinear behavior, as expected. Another significant contribution can be seen from the flexural component at level L2 which is located at the critical section of the column at the top of the sleeves. That was due the reasons mentioned in the previous section: existence of the critical section above the sleeve, strain penetration of column steel bars into the grouted sleeves and the increased deformation due to longitudinal bar debonding by the rubber cap at the top of the sleeve. This also explains why flexural deformation in level L2 for G-40-1 model is bigger than that in C-40-1 model although the level location is the same for both models. Flexural deformation contributions decrease above level L2. Flexural deformation at the mid-height of the sleeve (L1) exists but small. Flexural behavior above the sleeve shows a well-distributed flexural behavior that indicates a successful plastic hinge shifting. Shear deformation was approximately the same for both columns, implying that the effective aspect ratio had negligible effect on shear intensity for flexural-dominant columns.

For C-25-1 model, similar to C-40-1, the strain penetration in the footing contributes the most to the overall displacement observation of column models. Flexural contributions were similar to the patterns of C-40-1 model and shear deformation was little more than that in C-40-1. Contributions of displacement components for G-25-1 model were approximately similar to those in G-40-1 model. Strain penetration in the footing was significant but less than that in C-25-1 due to the elastic behavior of high-strength bars. The flexural component at level L2 (top of the sleeves) was another significant contribution to the total displacement for the same reasons explained in G-40-1 model. Like G-40-1 column, flexural deformation at the mid-height of the sleeve (L1) was small. However, the shear contribution appeared to be more than all other models, as was expected since the effective aspect ratio (L_{eff}/D) was reduced. The inclined shear cracks for this model were wider in width and caused gradual reduction in aggregate interlock with increasing drift ratios. That caused the shear strength to drop and thus affecting the lateral load capacity of the column (refer to the hysteresis loops of G-25-1 model). The plastic hinging for G-25-1 started to develop above the sleeve but shear degradation disrupted a well-defined plastic hinge.

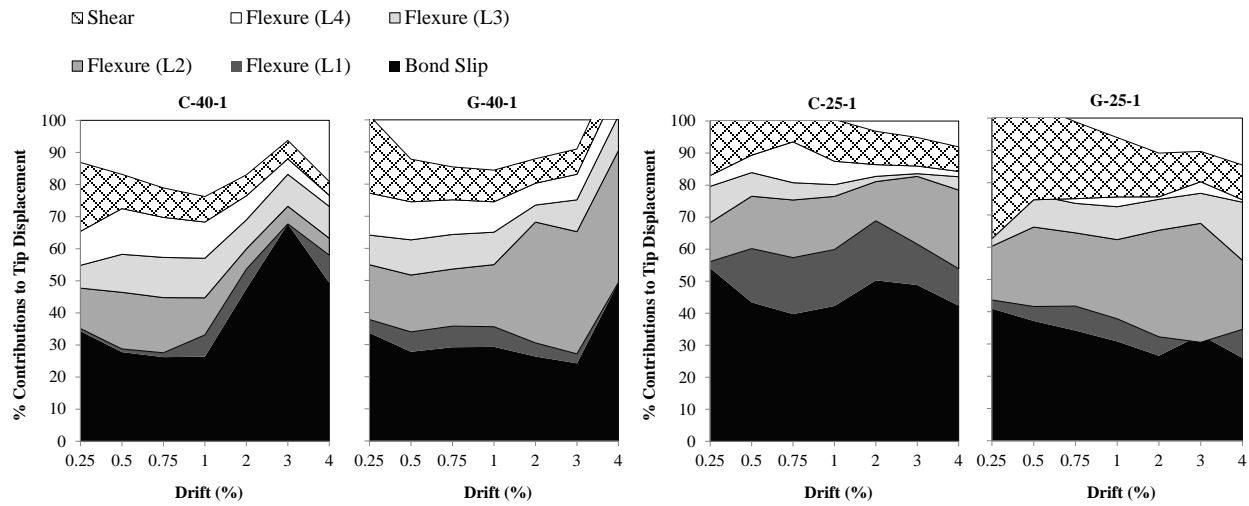


Fig. 12 – Displacement Components for the Columns

5. Conclusions

The primary goal of this research was to develop new design details for precast columns with grouted coupler connections for use in ABC in moderate to high seismic regions. A design detail using grouted coupler connections is proposed that improves the ductility and performance of the precast columns under lateral loads. Four 0.42-scale column models were designed, fabricated and tested. Performance indicators were force-displacement relationship, damage progression, energy dissipation and contributions of the displacement components.

The results indicate that shifted hinge design may be a very viable option for improving performance of flexural-dominant precast bridge columns with grouted coupler connections. Although there was a 16.5% reduction in lateral load-bearing capacity caused by a construction error, the force-displacement behavior of C-40-1 and G-40-1 were similar. The equivalent viscous damping ratio was 6% better for the precast column, which indicates that the precast column was able to dissipate more energy than the CIP column. A comparison of the damage progression showed how the plastic hinge formation is different for both columns, but both had similar failure modes and behaved according to expectations. Contributions of the lateral displacement components were in agreement with the apparent damage states. They also showed that the sleeve region cannot be neglected when designing precast columns with grouted couplers because the region exhibits rotation that contributes to the total column displacement. The displacement contributions also demonstrate the length of shifted plastic hinge cannot be predicted directly using existing equations for CIP columns.

The results of the columns with $AR = 2.5$ indicate that hinging occurred partially at the section above the grouted couplers prior to shear cracking/failure. The visual damage observations confirm the flexural cracking at lower drift levels followed by shear cracking and shear failure beyond 5% drift. The presence of the grouted sleeves caused reduced effective cantilever length. This, in turn, increased the shear intensity in the effective cantilever length and resulted in increased shear deformation and shear degradation. The flexural contributions to the column tip displacements showed that substantial flexural deformations continued to occur at all drift levels. It should be noted that many bridge columns have aspect ratios greater than 3. Therefore, testing of columns with $AR = 2.5$ was used to investigate an extreme case; however, further study of the shifted plastic hinge method for columns with shear-dominant behavior is warranted.

6. Acknowledgements

The authors express special thanks to Splice Sleeve Japan & North America for funding this research. The authors are also grateful for the assistance of MMFX Steel Corporation for donation of MMFX bars that were used in the research.

7. Copyrights

16WCEE-IAEE 2016 reserves the copyright for the published proceedings. Authors will have the right to use content of the published paper in part or in full for their own work. Authors who use previously published data and illustrations must acknowledge the source in the figure captions.

8. References

- [1] Marsh, M. L., Wernli, M., Garrett, B. E., Stanton, J. F., Eberhard, M. O., and Weinert, M. D. (2011) "Application of Accelerated Bridge Construction Connections in Moderate-to-High Seismic Region," NCHRP Report 698, 65 pp.
- [2] Haber, Z. B., Saiidi, M., and Sanders, D. H., (2013) "Precast Column-Footing Connection for Accelerated Bridge Construction in Seismic Zones," Center for Civil Engineering Earthquake Research, Department of Civil and Environmental Engineering, University of Nevada, Reno, Nevada, Report No. CCEER-13-08.
- [3] Ameli, M J., Parks, J. E., Brown D. N., and Partelides, C. P. (2015) "Seismic Evaluation of Grouted Splice Sleeve Connections for Reinforced Precast Concrete Column-to-Cap Beam Joints in Accelerated Bridge Construction," PCI Journal, March-April Issue, pp. 80-103.
- [4] Tazarv, M. and Saiidi, M., (2014) "Next Generation of Bridge Columns for Accelerated Bridge Construction in High Seismic Zones," Center for Civil Engineering Earthquake Research (CCEER), Department of Civil and Environmental Engineering, University of Nevada, Reno, Report No. CCEER-14-06.
- [5] Scribner, C. F. and Wight, J. K. (1978) "Delaying shear strength decay in reinforced concrete flexural members under large load reversals," Department of Civil Engineering, University of Michigan, Ann Arbor, Report UMEE 78R2.
- [6] Rutledge, S. T., Kowalsky, M. J., Seracino, R., & Nau, J. M. (2013) "Repair of reinforced concrete bridge columns containing buckled and fractured reinforcement by plastic hinge relocation," Journal of Bridge Engineering, V. 19, No. 8, A4013001.
- [7] Lehman, D. E., Gookin, S. E., Nacamuli, A. M., and Moehle, J. P. (March-April 2001) "Repair of Earthquake-Damaged Bridge Columns," ACI Structural Journal, V. 98, No. 2, pp. 233-242.
- [8] Parks, J. E., Brown, D. N., Ameli, M. J., Pantelides, C. P., and Reaveley, L. D. (2014) "Repair of Damaged Precast RC Bridge Columns with Grouted Splice Sleeve Connections Using CFRP Shells and Plastic Hinge Relocation," Proceedings of the Tenth U.S. National Conference on Earthquake Engineering, July 21-25, Anchorage, Alaska.
- [9] California Department of Transportations. (2013) "Seismic Design Criteria (SDC) Version 1.7," Division of engineering Services, Sacramento, CA.
- [10] Biskinis, D. E., Roupakias, G. K., & Fardis, M. N. (2004) "Degradation of shear strength of reinforced concrete members with inelastic cyclic displacements." ACI Structural Journal, V.101, No. 6, pp. 773-783.